Crystal structure and Mössbauer spectroscopy of the synthetic amphibole potassic-ferri-ferrorichterite at 298 K and low temperatures (80–110 K)

GÜNTHER J. REDHAMMER* and GEORG ROTH

Institute of Crystallography, Rheinisch-Westfälische-Technische Hochschule Aachen, Jägerstraße 17-19,
D-52056 Aachen, Germany
* mailing address: Neuhofen 224/1, A-4910 Ried im Innkreis, Austria
e-mail: redhammer@xtal.rwth-aachen.de

Abstract: The crystal structure of a synthetic potassic-ferri-ferrorichterite, ideally $K(Ca_{0.5}Na_{1.5})Fe_5Si_8O_{22}(OH)_2$ was refined from single-crystal X-ray imaging plate diffraction data at 298 K and 110 K. The title compound is monoclinic, S.G. $C2/m$, $Z = 2$, with a = 10.145(1) Å, b = 18.184(1) Å, c = 5.296(1) Å, β = 104.42(1)° at 298 K (sample Ri1). The structure is consistent with the general amphibole structure type. There is no crystallographic phase transition down to 110 K. The two nonequivalent T sites and the octahedral M1 and M3 sites behave very rigidly upon cooling. Bond lengths for the distorted M sites slightly decrease as temperature is lowered. The tetrahedral chain kinking increases by 0.9° between 298 K and 110 K. Similar behavior was found for a second sample investigated by single crystal X-ray diffraction. Mössbauer spectra, collected at 298 K, yield rather high ferric iron concentrations up to 2.0 a.p.f.u for the three samples investigated. Fe^{3+} prefers the M2 site. Three components were detected within the ferrous quadrupole splitting distribution (QSD) of the C-type sites and where assigned to the M1, M3 and M2 sites respectively. This assignment is consistent with polyhedral distortion and gives correct site occupancies. The magnitude of the quadrupole splitting of Fe^{2+} on M1 and M3 sites shows a dependency on the ferric iron content (mean cation radius of the M2 site) of the sample.

Key-words: crystal structure, Mössbauer spectroscopy, synthesis, amphibole, richterite.

Introduction

Amphiboles are a common group of complex rock-forming minerals which exhibit a wide range of chemical composition. They occur with orthorhombic and monoclinic symmetry and can accommodate cations of formal charge ranging from +1 to +4 and cationic radii from 0.25 to 1.61 Å (Hawthorne, 1982, 1983) into their general formula $A_{0-1}B_2C_5T_8O_{22}(OH,F,Cl)_2$.

Richterite, $Na(NaCa)Mg_5Si_8O_{22}(OH)_2$, is monoclinic, S.G. $C2/m$ and belongs to the subgroup of sodic-calcic amphiboles (Leake *et al.*, 1997). It occurs over a wide range of $P – T$ environments and is rather flexible with respect to cationic and/or anionic substitutions. It has been synthesized in several experimental studies (*e.g.*, Robert *et al.*, 1989; Raudsepp *et al.*, 1991, 1992; Gottschalk & Andrut, 1998 and references therein). Charles (1975) investigated the series richterite – ferrorichterite $Na(CaNa)(Mg_{5-x}Fe_x)Si_8O_{22}(OH)_2$, Sergent *et al.* (1997) examined (Fe,Mg) potassic richterites. Single-crystal structure refinements of richterites are rare. Papike *et al.* (1969) refined the structure of a natural potassic – richterite, Oberti *et al.* (1992) characterized Ti-bearing natural richterites, and Cameron *et al.* (1983) studied the high-temperature behavior of fluororichterite and potassic – fluororichterite. Very recently, Yang *et*

al. (1999) reported the single-crystal structure refinement of a K-substituted potassic – richterite $K(KCa)Mg_5Si_8O_{22}(OH)_2$. Structure refinements on various synthetic richterites using the Rietveld method were performed by Gottschalk & Andrut (1998), Robert *et al.* (1989, 1993), Della Ventura *et al.* (1993) and references in these papers. However structural investigations of ferrorichterites are not available up to now.

Only little is known about the Mössbauer spectra of sodic-calcic amphiboles. Virgo (1974) reports that the Mössbauer spectrum of synthetic ferrorichterite consists of two resolvable doublets due to Fe^{3+} and to Fe^{2+} and Sergent *et al.* (1997) describe the Mössbauer spectrum of a potassic – ferrorichterite. No other Mössbauer data are available.

Experimental details

Hydrothermal syntheses were done in cold-sealed, externally heated Tuttle-type pressure vessels operated at T = 600 or 700 °C and $P(H_2O)$ = 0.4 GPa. The tube-in-tube technique (Eugster & Wones, 1962) was applied to facilitate redox-condition control. Starting materials for synthesis were mixtures of K_2CO_3, Na_2CO_3, $CaCO_3$, Fe_2O_3 and SiO_2 in the stoichiometry of compositions $(K)(Na_{1+x}Ca_{1-x})Fe_5Si_8O_{22}(OH)_2$

Table 1. Synthesis experiments and results for potassic-ferri-ferro-richterite.

Run	T [°C]	P [kbar]	Buffer	t [h]	Result	Fe^{3+}/Fe_{tot}*
Ri1	700	4	NNO	450	cpx, ri	0.29
Ri10	600	2	NNO	213	ri	0.43
Ri15	600	2	MW	213	ri	0.19

T = temperature, P = pressure, t = time; NNO = nickel/ nickel oxide solid state buffer, MW = magnetite/ wuestite solid state buffer. Ri = richterite, cpx = clinopyroxene; * Fe^{3+}/Fe_{tot} ratio as determined by Mössbauer spectroscopy.

with x = 0 (Ri10) and x = 0.5 (Ri15). The starting material for sample Ri1 had the composition of the mixed valence pyroxene compound $Ca_{0.5}Na_{0.5}FeSi_2O_6$ (Redhammer *et al.*, 2000). Sodium carbonate used to prepare the starting material had a purity of 99.5 % containing < 0.02 % K by weight. Table 1 summarizes experimental conditions and results of syntheses. Run products were checked for amphibole yields optically and by X-ray powder diffraction.

The chemical analysis of the amphibole single crystals of run Ri1 and Ri15 were determined by means of electron microprobe (EMP) analysis using a JEOL JXA 8600, acceleration voltage of 15 kV, beam current of 30 nA, beam diameter focused to 3 μm. Larger amphibole crystals were embedded in epoxy-resin, polished, covered with carbon and analyzed. 20 points, rim – core – rim, were measured for each grain. Amphibole crystals of run Ri10 were too fine grained to be analyzed by EMP analysis.

Cell dimensions of amphiboles Ri1, Ri10 and Ri15 were determined by whole pattern refinement of X-ray powder diffraction data (10° – 120° 2θ, $CuK\alpha_{1,2}$ radiation) using Le Bail method implemented in FULLPROF (Rodrigues-Carvajal, 1998) at 298 K. Silicon was used as an internal standard.

Single-crystal X-ray diffraction data for samples Ri1 and Ri15 were collected on an image plate diffractometer (STOE-IPDS) system utilizing MoKα radiation and a pyrolytic graphite monochromator. The diffractometer was equipped with a cryostream liquid N_2 cryostat (110 K ... 300 K, accuracy 0.1 K). The programs X-SHAPE and X-RED (Stoe & Cie, 1996) for numerical absorption correction and SHELXS-86 and SHELXL-93 (Sheldrick, 1993) for structure solution and subsequent refinement were used.

The cell dimensions of sample Ri1 and Ri15 – as determined from the X-ray powder diffraction data at 298 K – were used as input for the single-crystal structure refinements of the corresponding single-crystal data sets as they are much more accurate than those determined from the single-crystal X-ray diffraction data. As we had no access to X-ray powder diffraction at low temperature (110 K), the cell dimensions at 110 K for sample Ri1 are from single-crystal X-ray diffraction data collection (Table 3).

The A-site potassium was assigned to the A(2/m) position (0, ½, 0, Hawthorne 1982). The T1 and T2 sites are fully occupied by Si, the M1, M2 and M3 sites by Fe, the M4 site by (Ca + Na) and the A site by (K + Na) for sample Ri1 and by K for Ri15. The ratio Ca/ Na and K/ Na was allowed to

vary during the refinement. The hydrogen atoms were detected from inspection of difference-Fourier peaks.

[57]Fe transmission Mössbauer spectra of the amphiboles Ri1, Ri10 and Ri15 were collected at 298 K using a Mössbauer apparatus in horizontal arrangement ([57]Co/Rh single line thin source, constant acceleration, symmetric triangular velocity shape, multi-channel analyzer with 1024 channels, velocity calibration to α-Fe). For sample Ri1, a Mössbauer spectrum was recorded at 80 K also using a bath cryostate. For Mössbauer absorber preparation, samples were carefully ground under ethanol (to avoid oxidation), mixed with powder sugar and filled into Cu-rings (inner diameter 10 mm), covered with a high purity Al-foil on one side. This preparation method produces absorbers free of preferred orientation effects. To test for preferred orientation effects, we have also recorded Mössbauer spectra oriented with an angle of 54° to the incident γ-ray but found no differences to those with the absorber oriented at right angle. The folded spectra were analyzed with the Voigt-function based quadrupole splitting distribution method (Rancourt & Ping, 1991; Rancourt *et al.*, 1996) implemented in the program suite RECOIL. Complete thickness correction was applied to all Mössbauer data (Rancourt *et al.*, 1993).

Results

Synthesis and mineral chemistry

Amphibole crystals up to 500 μm in diameter (sample Ri1) grew on one side of the long Au-tube in the temperature gradient of the pressure vessel during an experiment to crystallize the mixed valence pyroxene compound $Ca_{0.5}Na_{0.5}FeSi_2O_6$ (*cf.* Redhammer *et al.*, 2000). Electron-microprobe analysis yielded the following chemical composition:
$[K_{0.90(2)}Na_{0.06(2)}]$ $[Ca_{0.58(1)}Na_{1.36(2)}Fe^{2+}_{0.06(2)}]$ $[Fe^{2+}_{3.48(2)}Fe^{3+}_{1.52(2)}]$ $Si_{7.99(1)}O_{22}(OH)_2$
based on 24 anions. The valency of iron was determined from the results of Mössbauer spectroscopy. The potassium in the amphibole was derived from the sodium carbonate in which 0.02 wt.% of K is present.
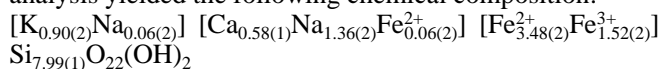
Synthesis experiments to grow amphibole products of composition $(K)(Na_{1+x}Ca_{1-x})(Fe_5)Si_8O_{22}(OH)_2$, x = 0.0, and 0.5 from stoichiometric starting materials and under controlled conditions gave single-phase run products (Table 1). Potassic-ferri-ferrorichterite with x = 0.0 (Ri10) yield a fine-grained single-phase product (grain sizes < 0.005 mm); for x = 0.5, large crystals up to 0.3 mm (Ri15) grew. For the latter sample, it was possible to determine the chemical composition by electron microprobe analysis. This yielded the following structural formula:
$[K_{0.90(1)}Na_{0.10(6)}]$ $[Ca_{0.52(4)}Na_{1.48(2)}]$ $[Fe^{2+}_{3.50(2)}Fe^{3+}_{1.50(1)}]$ $Si_{7.99(1)}O_{22}(OH)_2$
based on 24 anions and the results of Mössbauer spectroscopy. This shows the sample to be of the desired composition except a small amount of sodium at the A-site. A very similar composition also was found for the sample Ri1. There is a slight variation in the Na_2O-CaO contents from grain to grain analyzed. The Ca^{2+} contents determined are between 0.46 and 0.59 atoms per formula unit and are highly corre-
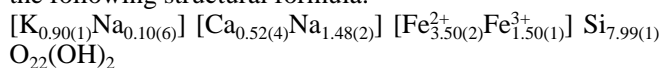
(a)

(b)

(c)

Fig. 1. Mössbauer spectrum of sample Ri1, collected at 298 K (a), corresponding trimodal Fe^{2+} quadrupole splitting distribution curve at 298 K (b) as extracted from the spectrum shown in (a) and Mössbauer spectrum of sample Ri1, collected at 80 K (c).

Table 2a. ^{57}Fe Mössbauer fit parameter for thickness – corrected spectra of synthetic potassic-ferri-ferrorichterites samples Ri1, Ri10 and Ri15 at 298 K and 80 K (Ri1).

	Temp. [K]	δ [mm/s]	Δ [mm/s]	σ_Δ [mm/s]	Area [%]	site
Ri1	298	1.15(2)	2.79(3)	0.09(1)	36.9(9)	Fe^{2+} M1
		1.16(2)	2.37(3)	0.12(1)	16.4(9)	Fe^{2+} M3
		1.17(2)	1.93(3)	0.15(1)	15.5(9)	Fe^{2+} M2
		1.134(4)	1.43(5)	0.06(1)	2.3(9)	Fe^{2+} M4
		0.42(2)	0.45(2)	0.12(1)	29.9(7)	Fe^{3+} M2
		0.42(2)	1.17(5)	0.10(1)	2.0(7)	Fe^{3+} M3
		0.43(2)	1.70(4)	0.07(3)	3.0(7)	Fe^{3+} M1
Ri1	80	1.26(1)	3.13(4)	0.12(1)	37.0(9)	Fe^{2+} M1
		1.27(1)	2.80(4)	0.15(3)	17.2(9)	Fe^{2+} M3
		1.27(1)	2.56(8)	0.42(5)	15.3(9)	Fe^{2+} M2
		1.15(6)	1.64(9)	0.12*	2.3(6)	Fe^{2+} M4
		0.51(2)	0.46(3)	0.15(1)	22.6(8)	Fe^{3+} M2
		0.51(2)	0.5(1)	0.12(1)	2.8(8)	Fe^{3+} M3
		0.51(2)	0.99(4)	0.11(2)	2.8(8)	Fe^{3+} M1
Ri10	298	1.14(1)	2.57(2)	0.15(2)	39.2(5)	Fe^{2+} M1
		1.13(1)	2.11(2)	0.28(1)	18.2(5)	Fe^{2+} M3
		0.36(1)	0.40(1)	0.22(1)	40.1(4)	Fe^{3+} M2
		0.36(1)	1.26(2)	0.24(2)	2.5(4)	Fe^{3+} M3
Ri15	298	1.15(1)	2.85(4)	0.15(1)	38.8(6)	Fe^{2+} M1
		1.14(1)	2.66(5)	0.11(1)	17.0(6)	Fe^{2+} M3
		1.14(1)	2.17(3)	0.36(2)	25.1(6)	Fe^{2+} M2
		0.39(1)	0.49(1)	0.22(2)	15.4(5)	Fe^{3+} M2
		0.39(1)	1.14(4)	0.12(1)	1.4(5)	Fe^{3+} M3
		0.39(1)	1.58(4)	0.12(1)	2.3(5)	Fe^{3+} M1

* All fits impose $\Gamma = 0.194$ mm/s and h-/h+ = 1; isomer shift δ is taken to be correlated to their quadrupole splitting Δ by $\delta = \delta_o + \delta_1$, reduced χ^2_{red} values are 0.699, 0.571 and 1.299 and 0.60 for Ri1 (298 K), Ri1 (80 K), Ri10 and Ri15 respectively.

constant as well as the potassium, iron and silicon contents are remarkably constant for all grains analyzed.

Mössbauer spectroscopy

The 298 K ^{57}Fe Mössbauer spectrum of powdered potassic-ferri-ferrorichterite single crystals of sample Ri1 is shown in Figure 1a, ^{57}Fe Mössbauer fit parameters are included in Table 2a. The spectrum exhibits evidence for Fe^{3+} in octahedral coordination indicated by the pronounced and well-resolved peak at ≈ 0.6 mm/s. The high velocity peak, which is solely due to Fe^{2+} shows a well-developed shoulder at low Doppler-velocities, indicative of at least two Fe^{2+} components. For the initial refinements, a quadrupole splitting distribution model with two generalized sites f_2 (for Fe^{2+}) and f_3 (for Fe^{3+}) was chosen. Appropriate refinements can be obtained with one ferric ($\Delta=0.42$ mm/s) and two ferrous components ($\Delta=2.78$ and 2.26 mm/s) contributing to f3 and f2 respectively. The two ferrous components are equal in integrated intensity (35 % of total iron each) and the Fe^{3+}/Fe_{tot} ratio is 0.29. However, distinct amounts of residual resonance absorption is observed at ≈ 1.1 mm/s, which is indica-

lated with the Na^+ content, *i.e.* higher Ca^{2+} contents are related to lower Na^+ contents on the M4 site, the amount of Na^+, which has to be placed on the A site, however, stays

Table 2b. Site populations at C-type sites as calculated from Mössbauer spectroscopic results.

	M1		M2		M3		M4[§]		
	Fe^{2+}	Fe^{3+}	Fe^{2+}	Fe^{3+}	Fe^{2+}	Fe^{3+}	Fe^{2+}	Ca^{2+}	Na^+
Ri1, 298 K	1.88(2)	0.10(2)	0.79(2)	1.22(2)	0.84(2)	0.15(2)	0.06*	0.55(1)	1.39(1)
Ri1, 80 K	1.89(3)	0.15(3)	0.78(3)	1.15(3)	0.88(3)	0.15(3)	0.06*	0.57(1)	1.37(2)
Ri15	1.94(3)	0.07(2)	1.25(3)	0.77(2)	0.85(3)	0.11(2)	---	0.52(1)	1.48(1)
Ri10	1.96(3)	---	---	2.01(2)	0.91(3)	0.13(2)	---	n.d.	n.d.

[§] M4 site population from single crystal structure refinement of X-ray diffraction data. Site occupation of Fe^{2+} at M4 was fixed according to electron microprobe analysis during structure refinement. Mössbauer spectroscopic results yield 0.12(4) atoms Fe^{2+} on M4 at 298 K and 80 K respectively.

* value fixed during structure refinement.

tive for an additional Fe^{2+} component and problems arise in assignment of Fe^{2+} to the M sites. Furthermore, some residual resonance absorption is also observed for ferric iron, indication that Fe^{3+} occupies more than one M site.

The best refinements are obtained using three Fe^{3+} and three Fe^{2+} components contributing to f_3 and f_2, respectively. Throughout this procedure, the Fe^{3+}/Fe_{tot} ratio remains at 0.29. According to Hawthorne (1982), trivalent cations prefer the M2 site in amphiboles. Thus the most intense Fe^{3+} component with Δ=0.45 mm/s was assigned to the M2 site. The two other Fe^{3+} components with Δ=1.17 and Δ=1.70 mm/s are weak in intensity (2 % and 3 % of total iron respectively) and are assigned to the M3 and M1 site. This gives reasonable site occupancies (Table 2b). The presence of the two additional Fe^{3+} components is justified by the presence of two weak but visually detectable shoulders in the Mössbauer spectrum in the range of 0.0 – 0.8 mm/s and by statistical reasons as reduced χ^2 is lowered significantly (0.97 to 0.60).

The ferrous quadrupole splitting distribution curve is shown in Figure 1b. It exhibits rather well resolved probability density maxima at 2.79, 2.37 and 1.93 mm/s. As there is no extensive overlap of the three ferrous components of the generalized site f_2, they are assigned to specific crystallographic C-type M sites. Based on literature data for actinolite (Burns & Greaves, 1971) and the assumption of a negative correlation between Fe^{2+} quadrupole splitting and the distortion from ideal octahedral geometry (Ingalls, 1964; Dowty & Lindsley, 1973) the following site assignment was done: the component with highest quadrupole splitting (Δ = 2.77) is assigned to Fe^{2+} at the M1 site, the one with Δ=2.31 mm/s to Fe^{2+} at M3 and finally the component with lowest QS of Δ=1.80 mm/s to Fe^{2+} at the M2 site. Finally, we found evidence for the presence of a fourth ferrous component, weak in intensity. It was introduced as an own site, named f_4 and is assigned to Fe^{2+} on the B-type M4 site. Microprobe analysis also gives evidence for some Fe^{2+} on M4. The site assignment proposed here is in contrast to Sergent *et al.* (1997) but in concordance with polyhedral distortion of M sites. Furthermore, this Fe^{2+} site assignment gives reasonable Fe populations (Table 3) at the C-type sites. Figure 1c shows the ^{57}Fe Mössbauer spectrum of sample Ri1 recorded at 80 K. At low temperatures, the Fe^{2+} components become more overlapped and resolution of individual Fe^{2+} sites is difficult. Cooling down to low temperatures thus does not help to increase spectral resolution. However, the Fe^{3+}/Fe

ratio is the same at 298 K and 80 K within experimental error.

The 298 K ^{57}Fe Mössbauer spectrum of the potassic-ferri-ferrorichterite Ri10, ideally $K(NaCa)Fe_5Si_8O_{22}(OH)_2$, grown at the oxidizing redox conditions of the NNO solid state buffer is shown in Figure 2a. The f_3 site is built up by a domination component with Δ=0.40 mm/s, assigned to the M2 site and an additional weak component (arrow in Figure 2a) with Δ=1.26 mm/s, assigned to the M3 site in analogy to sample Ri1. The Fe^{3+}/Fe_{tot} ratio is 0.43. The M2 site is exclusively filled by Fe^{3+}. The generalized site f_2 consists of two components. No additional shoulders are visible. The two f_2 components are centered at 2.57 (M1) and 2.11 mm/s (M3) with relative area ratios of 68.3(8) % and 31.7(8) % of total Fe^{2+} respectively. The proposed site assignment gives rise to reasonable site populations for iron at the C-type sites, which agree well with the maximal possible occupation of these sites within experimental error. The refinement of the Mössbauer spectrum of the Ri10 potassic-ferri-ferrorichterite gives evidence for a strong preference of Fe^{3+} for the M2 position and further supports the assignment of individual ferrous components to the crystallographic M1, M2 and M3 sites.

Figure 2b shows the 298 K ^{57}Fe Mössbauer spectrum of sample Ri15, which has a similar composition to Ri1; it however was synthesized at the redox conditions of the MW solid state buffer. Ri15 shows less Fe^{3+} and the ferrous QSD is less resolved as compared to Ri1. In Ri15, the three components contributing to f_2 are centered at higher quadrupole splittings, namely 2.85, 2.66 and 2.17 mm/s for M1, M3 and M2 respectively. As what concerns the Ri15 sample, the extraction of site-occupancy numbers becomes somewhat problematic, as there is no longer a clear separation between the M1 and M3 resonance absorption contribution. The main difference between sample Ri1 and Ri15 is the concentration of ferric iron, located on the M2 site. This hints that the ferric (trivalent) cation content has an influence on the size of the ferrous quadrupole splittings. This is what actually happens.

Hawthorne (1983) noted the quadrupole splitting at M3 to be sensitive to the mean ionic radius on the M2 site for alkali amphiboles. He observed a positive correlation between Fe^{2+} at M3 quadrupole splitting and the mean ionic radius of the M2 cation whereas he did not find a similar correlation for the M1 site. The data of this study give evidence, that the above-mentioned positive correlation also holds

Table 3. Cell dimensions of synthetic potassic-ferri-ferrorichterite from powder X-ray diffraction at 298 K.

	Ri1 298 K *	Ri1 298 K**	Ri1 110 K **	Ri15*￼	Ri15**	Ri10*
a_0 [Å]	10.1448(10)	10.144(3)	10.1306(25)	10.1361(9)	10.134(3)	10.1341(9)
b_0 [Å]	18.1841(10)	18.195(4)	18.1678(29)	18.1648(10)	18.174(4)	18.1741(9)
c_0 [Å]	5.2962(8)	5.302(2)	5.2889(13)	5.3030(7)	5.305(2)	5.3049(7)
β	104.415(6)	104.5(1)	104.54(29)	104.327(6)	104.5(1)	104.506(6)
V [Å³]	946.26	947.42	942.27	946.02	945.93	945.90

* from X-ray powder diffraction, ** from X-ray single crystal structure refinement.
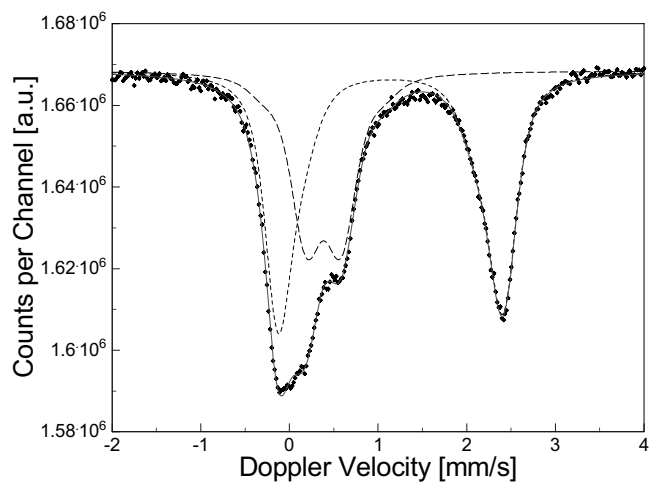
(a)
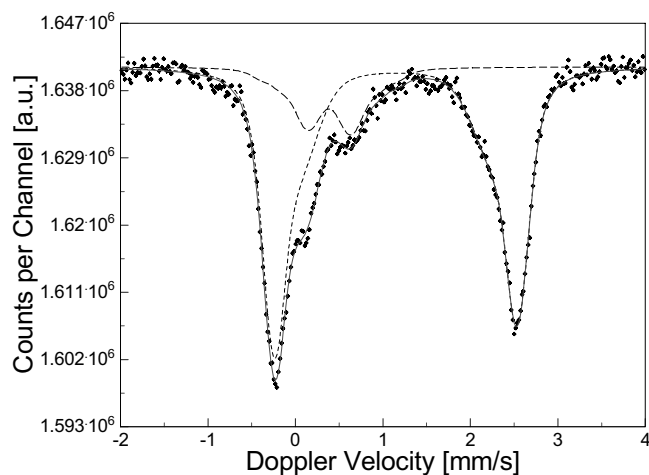
(b)

Fig. 2. ^{57}Fe Mössbauer spectra of samples Ri10 (a) and Ri15 (b) collected at 298 K.

true for the M1 site. Figures 3a – b compile quadrupole splitting values of Fe^{2+} at the M1 and M3 sites of calcic, sodic-calcic and alkali amphiboles plotted *versus* the mean M2 ionic radius. The M1 and M3 quadrupole splitting values for Fe^{2+} of this study decrease with increasing Fe^{3+} content (decreasing mean ionic radius) at the M2 site. Thereby, the quadrupole splitting of Fe^{2+} at the M3 sites, sharing edges with two neighboring M2 sites, seems to be more sensitive to changes in Fe^{3+} concentrations at M2 (Figure 3c). Assum-

ing a linear correlation between ferrous quadrupole splitting and mean M2 ionic radius, one might speculate that for amphiboles having exclusively ferrous iron at the M1, M2 and M3 sites the difference between M1 and M3 ferrous quadrupole splitting would be less than 0.1 mm/s. For this case, M1 and M3 sites can not be differentiated from each other any more. This might also hold true for amphiboles with low Fe^{3+} concentrations ($Fe^{3+}/Fe_{tot} < 0.1$).

Structure refinement

Cell dimensions, details of data collection, atomic coordinates and selected bond lengths and bond angles are compiled in the Tables 3 – 6. The structure of potassic-ferri-ferrorichterite is in close agreement with literature data (*e.g.* Papike *et al*., 1969, Cameron *et al*., 1983, Yang *et al*., 1999). For a general description of amphibole topologies see *e.g.* Hawthorne (1983).

Table 4. Crystal and structure refinement data for potassic-ferri-ferrorichterite

Sample Temperature	Ri1 298 K	Ri1 110 K	Ri15 298 K
Wavelength	0.71073	0.71073	0.71073
Space group	*C*2/m	*C*2/m	*C*2/m
Z	2	2	2
Density (calc)	3.398	3.407	3.384 g/cm³
Absorption coefficient	4.709	4.709	4.68 mm⁻¹
F(000)	897	897	897
Index range	$-13 \le l \le 13$	$-13 \le l \le 13$	$-13 \le l \le 13$
	$-24 \le k \le 23$	$-24 \le k \le 23$	$-23 \le k \le 23$
	$-6 \le h \le 6$	$-6 \le h \le 6$	$-6 \le h \le 6$
Reflections collected	6091	5203	4679
Unique reflections	1150	1173	1170
R_{int}	0.022	0.035	0.0372
refined parameters	105	105	105
GOF	1.097	1.098	1.114
R_1 [I > 4σ]	0.0175	0.0212	0.0207
wR_2 [I > 4σ]	0.0487	0.0471	0.0491
R_1 all data	0.0214	0.0344	0.0304
wR_2 all data	0.0576	0.0597	0.0594
Difference	0.41/ -0.37	0.59/ -0.46	0.57/ -0.39 e/Å³

Table 5. Fractional atomic coordinates and isotropic atomic displacement parameters [Å²] for potassic-ferri-ferrorichterite Ri1 (298 K, 110 K) and Ri15 (298 K).

Atom	x	y	z	U_{eq}
Ri 1, T = 298 K:				
Si(1)	0.27313(4)	0.08520(2)	0.29382(7)	0.0038(1)
Si(2)	0.28545(3)	0.17036(2)	0.80106(7)	0.0043(1)
Fe(1)	0	0.09184(1)	½	0.0072(1)
Fe(2)	0	0.18382(1)	0	0.0071(1)
Fe(3)	0	0	0	0.0070(1)
M(4)	0	0.27738(3)	½	0.0141(2)
O(1)	0.1104(1)	0.08950(5)	0.2103(2)	0.0062(2)
O(2)	0.1216(1)	0.17299(5)	0.7273(2)	0.0075(2)
O(3)	0.1061(2)	0	0.7083(3)	0.0080(3)
H	0.192(5)	0	0.761(8)	0.05(1)
O(4)	0.3643(1)	0.24520(5)	0.7962(2)	0.0100(3)
O(5)	0.3415(1)	0.12755(5)	0.0866(2)	0.0087(2)
O(6)	0.3365(1)	0.11610(5)	0.5871(2)	0.0090(2)
O(7)	0.3257(1)	0	0.2964(3)	0.0088(3)
A(2/m)	0	½	0	0.0391(2)
Ri 1, T = 110 K:				
Si(1)	0.27347(6)	0.08524(3)	0.29470(13)	0.0008(1)
Si(2)	0.28572(6)	0.17042(3)	0.8018(1)	0.0010(1)
Fe(1)	0	0.09176(2)	½	0.0029(1)
Fe(2)	0	0.18351(2)	0	0.0031(1)
Fe(3)	0	0	0	0.0028(1)
M(4)	0	0.27716(5)	½	0.0054(4)
O(1)	0.1103(2)	0.08944(7)	0.2102(3)	0.0021(3)
O(2)	0.1210(2)	0.17299(7)	0.7276(3)	0.0030(3)
O(3)	0.1058(2)	0	0.7084(4)	0.0031(4)
H	0.189(5)	0	0.75(1)	0.01(1)
O(4)	0.3642(2)	0.24551(8)	0.7951(3)	0.0042(3)
O(5)	0.3423(2)	0.12828(8)	0.0891(3)	0.0033(3)
O(6)	0.3369(2)	0.11572(8)	0.5889(3)	0.0028(3)
O(7)	0.3266(2)	0	0.2954(4)	0.0035(4)
A(2/m)	0	½	0	0.0168(5)
Ri 15, T = 298 K:				
Si(1)	0.27264(5)	0.08535(2)	0.29418(9)	0.0034(1)
Si(2)	0.28523(5)	0.17043(3)	0.80135(9)	0.0038(1)
Fe(1)	0	0.09181(2)	½	0.0070(1)
Fe(2)	0	0.18397(2)	0	0.0067(1)
Fe(3)	0	0	0	0.0075(1)
M(4)	0	0.27751(5)	½	0.0128(4)
O(1)	0.1102(1)	0.08988(7)	0.2104(3)	0.0061(3)
O(2)	0.1212(1)	0.17308(7)	0.7283(3)	0.0074(3)
O(3)	0.1058(2)	0	0.7084(4)	0.003(1)
H	0.15(1)	0	0.70(2)	0.03(2)
O(4)	0.3642(1)	0.24536(7)	0.7971(3)	0.0094(3)
O(5)	0.3414(1)	0.12746(7)	0.0868(3)	0.0077(3)
O(6)	0.3363(1)	0.11632(7)	0.5871(3)	0.0080(3)
O(7)	0.3246(2)	0	0.2979(4)	0.0082(4)
A(2/m)	0	½	0	0.0355(5)

Table 6. Selected interatomic distances [Å] and angles [°] in synthetic potassic-ferri-ferrorichterite Ri1 (298 K, 110 K) and Ri15 (298 K). Estimated standard deviations are smaller than 0.003 Å for bond lengths and 0.09° for bond angles.

M1 site	Ri1	Ri1 (110)	Ri15
M1-O2 x2	2.100	2.095	2.102
M1-O1 x2	2.113	2.112	2.111
M1-O3 x2	2.139	2.133	2.139
<M1-O>	2.117	2.113	2.117
O-O distances:			
O1-O3 x2	2.851	2.845	2.850
O1-O3 x2	3.110	3.106	3.114
O1-O2 x2	2.888	2.880	2.875
O1-O2 x2	3.108	3.106	3.112
O2-O2	2.989	2.975	2.993
O3-O3	2.674	2.661	2.678
O2-O3 x2	3.150	3.147	3.148
<O-O>	2.990	2.983	2.989
O-M1-O bond lengths:			
O1-O1	177.70	177.71	178.09
O1-O2 x2	86.55	86.39	86.09
O1-O2 x2	95.07	95.23	95.25
O1-O3 x2	84.20	84.16	84.25
O1-O3 x2	94.00	94.04	94.26
O2-O2	90.71	90.45	90.78
O3-O3	77.36	77.18	77.53
O2-O3 x2	95.98	96.20	95.86
O2-O3 x2	173.21	173.27	173.29
BLD [%]	0.68	0.62	0.68
ELD [%]	8.85	8.86	8.87
OAV [°]	33.43	34.32	33.73
M2 site	**Ri1**	**Ri1 (110)**	**Ri15**
M2-O4 x2	1.997	1.996	1.992
M2-O2 x2	2.130	2.122	2.122
M2-O1 x2	2.194	2.187	2.190
<M2-O>	2.107	2.102	2.101
O-O distances:			
O2-O4 x2	2.902	2.898	2.893
O2-O4 x2	3.105	3.091	3.097
O2-O1 x2	2.888	2.880	2.875
O2-O1 x2	3.002	2.995	2.996
O1-O1	2.738	2.729	2.739
O4-O4	3.047	3.046	3.047
O1-O4 x2	3.018	3.011	3.005
<O-O>	2.968	2.960	2.960
O-M2-O bond angles:			
O1-O1	77.19	77.20	77.40
O1-O2 x2	83.80	83.86	83.63
O1-O2 x2	87.91	88.06	88.01
O1-O4 x2	92.00	91.96	91.75
O1-O4 x2	167.35	167.39	167.21
O2-O2	169.39	169.67	169.29
O2-O4 x2	89.33	89.41	89.31
O2-O4 x2	97.54	97.28	97.60
O4-O4	99.44	99.48	99.76

Table 6. (cont.)

M2 site	Ri1	Ri1 (110)	Ri15
BLD [%]	*3.48*	*3.35*	*3.47*
ELD [%]	*8.69*	*8.69*	*8.70*
OAV [°]	*63.86*	*62.55*	*64.83*
M3 site	Ri1	Ri1 (110)	Ri15
M3-O3 x2	2.090	2.087	2.090
M3-O1 x4	2.127	2.122	2.131
<M3-O>	*2.115*	*2.110*	*2.117*
O-O distances:			
O1-O3 x4	2.851	2.845	2.850
O1-O3 x4	3.107	3.103	3.114
O1-O1 x2	2.738	2.729	2.739
O1-O1 x2	3.255	3.250	3.265
<O-O>	*2.985*	*2.979*	*2.989*
O-M3-O bond angles:			
O1-O1 x2	180.00	180.00	180.00
O1-O1 x2	80.13	80.04	79.98
O1-O1 x2	99.87	99.96	100.02
O1-O3 x4	85.06	85.03	84.94
O1-O3 x4	94.94	94.97	95.06
O3-O3	180.00	180.00	180.00
BLD [%]	*0.78*	*0.74*	*0.86*
ELD [%]	*5.76*	*5.80*	*5.87*
OAV[°]	*41.78*	*42.46*	*43.32*
M4 site	Ri1	Ri1 (110)	Ri15
M4-O4 x2	2.367	2.361	2.371
M4-O2 x2	2.416	2.407	2.416
M4-O5 x2	2.664	2.67	2.658
M4-O6 x2	2.935	2.913	2.936
<M4-O>	*2.596*	*2.588*	*2.595*
BLD [%]	*7.860*	*7.874*	*7.774*
A site	Ri1	Ri1 (110)	Ri15
A-O5 x4	2.923	2.930	2.919
A-O6 x4	3.191	3.174	3.196
A-O7 x2	2.641	2.628	2.641
A-O7 x2	3.706	3.700	3.700
<A-O>	*3.096*	*3.089*	*3.099*
T1 site	Ri1	Ri1 (110)	Ri15
Si-O1	1.602	1.602	1.598
Si-O6	1.626	1.624	1.628
Si-O5	1.630	1.631	1.631
Si-O7	1.637	1.639	1.636
<Si-O>	*1.624*	*1.624*	*1.623*
T2 site	Ri1	Ri1 (110)	Ri15
Si-O4	1.582	1.584	1.582
Si-O2	1.610	1.616	1.611
Si-O5	1.670	1.669	1.673
Si-O6	1.679	1.678	1.678
<Si-O>	*1.635*	*1.637*	*1.636*

BLD (bond lengths distortion) and ELD (edge length distortion according to Renner & Lehmann (1986). OAV (octahedral angle variance) according to Robinson *et al*. (1971).

(a)

(b)

(c)
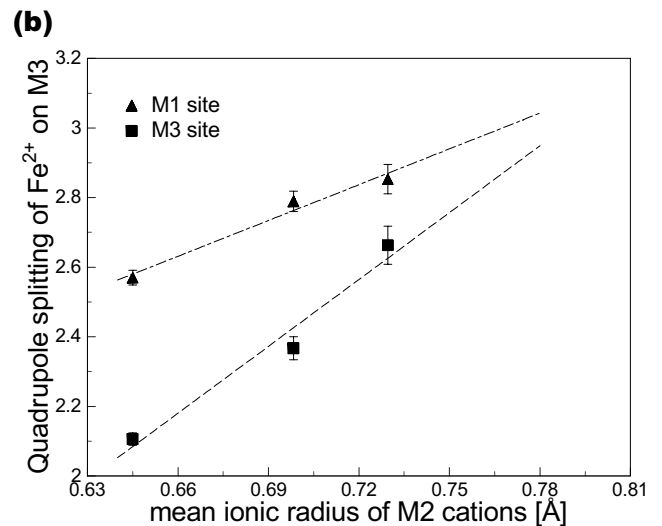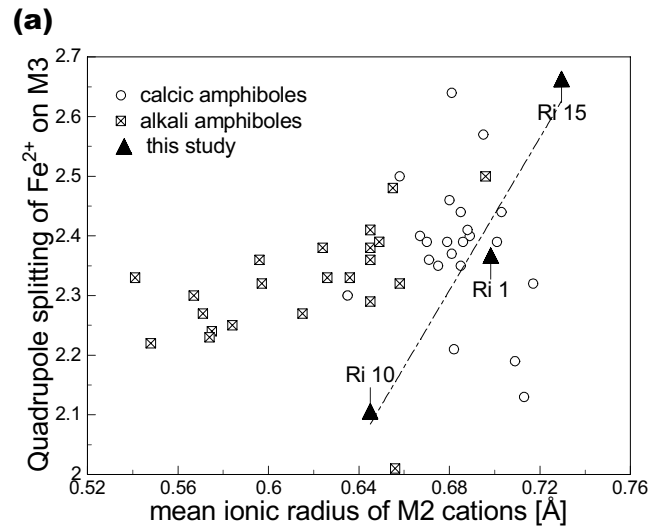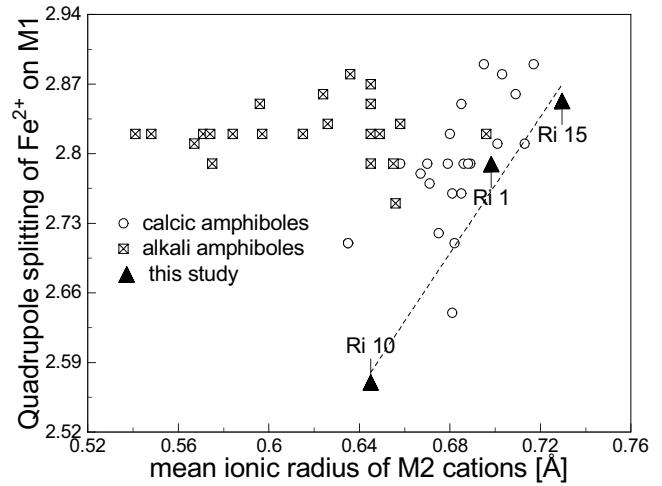
Fig. 3. Variation of the Fe^{2+} quadrupole splitting [in mm/s] on M1 (a) and M3 (b) for samples Ri1, Ri10 and Ri15 of this study, compared to data taken from the literature (Bancroft & Burns, 1969; Ernst & Wai, 1970; Burns & Greaves, 1971; Bancroft & Brown, 1975; Appendix F from Hawthorne, 1983); linear regressions were fitted to the data of this study as eye-guides (c).

The interatomic distances <Si-O> within the double chain of tetrahedra are similar in both samples studied here. Upon cooling, the tetrahedral sites behave rigidly and no significant changes were observed in Si-O bond lengths and in O-Si-O bond angles. There is a small increase in the kinking of tetrahedral chains, expressed by the smaller O5-O6-O5 angle of 169.87(8)° as compared to the value at 298 K with 170.76(8)°.

The M1, M2 and M3 octahedra are exclusively occupied by iron in the samples studied here. The M1 and the M3 sites are coordinated by four oxygens and two hydroxyl groups in cis and trans positions, respectively. Both octahedra have similar <M-O> bond lengths (Table 6) and bond lengths distortion parameters (BLD). The quadratic octahedral angle variance (OAV) however is smaller on the M1 site as compared to the M3 site ($\approx$ 32.8° and 42.8° on M1 and M3 respectively). The M2 cation is coordinated by six oxygens. Individual M2-O interatomic distances range between 1.997 Å and 2.194 Å, (sample Ri1, Table 6), the bond lengths as well as the angular distortion are large. In terms of bond lengths distortion and octahedral angle variance, the M1 oxygen atom octahedron is the most regular one, the M2 the most distorted one. The M3 oxygen octahedron deviates slightly from the ideal octahedral geometry as does the M1 site. Oxygen octahedra are rather similar to each other in terms of <M-O> bond lengths and distortion parameters in samples Ri1 and Ri15. Only the M3 sites exhibit a slightly larger quadratic octahedral angle variance in sample Ri15 as does the corresponding one in sample Ri1. Mean and individual bond lengths of M1 and M3 in both samples investigated here are systematically longer by 0.05 – 0.07 Å as compared to the mainly Mg^{2+} bearing natural (Papike *et al.*, 1969) and synthetic potassium richterites (Cameron *et al.*, 1983, Yang *et al.*, 1999). In Figure 4 the <M-O> bond lengths of the two samples Ri1 and Ri15 (at 298 K) are compared with data from the literature. The mean ionic radii for samples Ri1 and Ri15 are calculated based on the results of Mössbauer spectroscopy. For all calculations, ionic radii given by Shannon & Prewitt (1969) and Shannon (1970) were used. As can be seen, the data of the potassic-ferri-ferrorichterites plot well into the general trend observed for the relationship between <M-O> and mean ionic radius of the specific M-site cation. Only the <M2-O> bond lengths of sample Ri1 slightly falls off the general trend.

With decreasing temperature, the <M-O> decrease by 0.004 – 0.005 Å. The Fe1-O3 and the Fe2-O1, O2 bond lengths show the largest shortenings. The O-O interatomic distances (edges of the octahedra) also become shortened. However, the bond length distortion (BLD) as well as the edge lengths distortion (ELD) remain rather unaffected by cooling. The octahedral angle variance increases by less than 1° for M1 and M3 and decreases by more than 1° for the M2 site.

The M4 site is located at the junction of the octahedral strip and the tetrahedral chains. Refined site population for sample Ri1 agree well with chemical analysis (Table 2a). The coordination of the M4 site can be divided into four short bonds (2.368 – 2.422 Å) and four longer bonds ($\approx$ 2.67 Å, $\approx$ 2.93 Å). The latter ones are those linking the octahedral strip and the tetrahedral chains. The M4 site is the most dis-

(a)

(b)

(c)
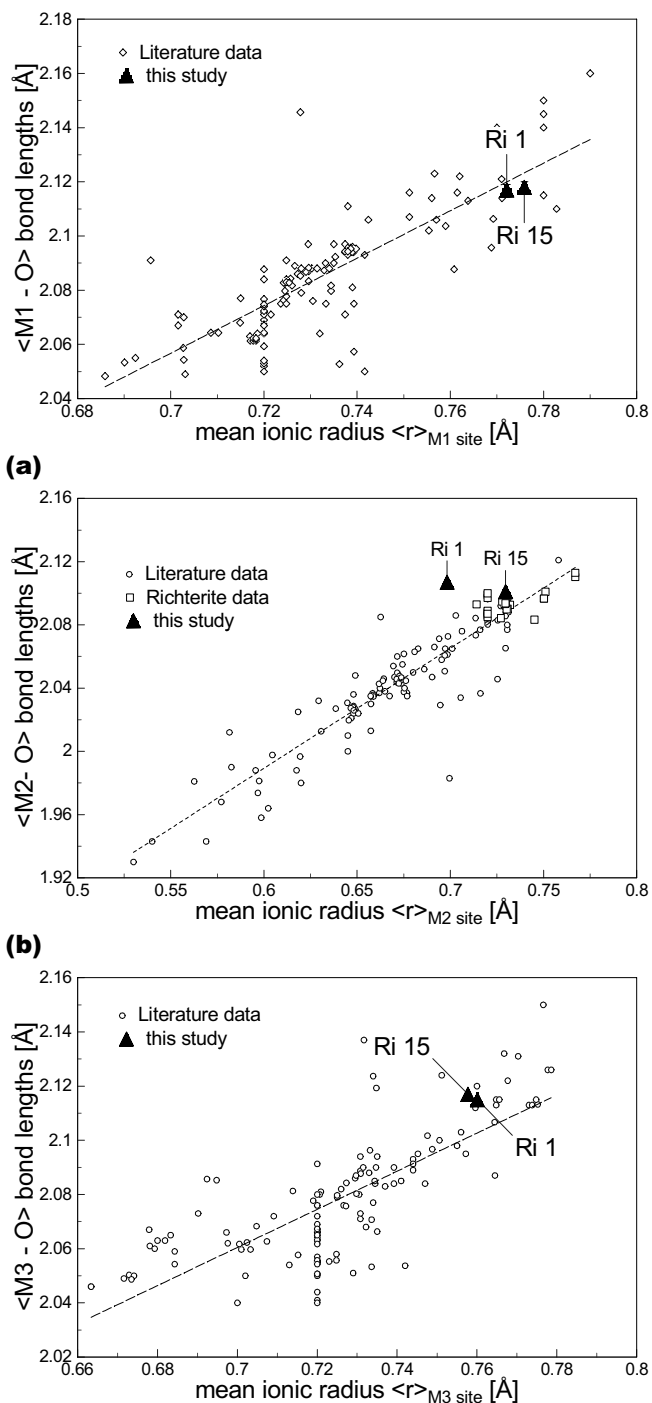
Fig. 4. Relationship between mean ionic radii and <M-O> bond length for the M1, M2 and M3 sites of *C*2/*m* amphiboles. Data of this study for samples Ri1 and Ri15 are compared with literature data. (Hawthorne, 1983; Inorganic crystal structure database ICSD, release 2000/1). Dashed lines are linear regressions and should serve as guides to the eye.

torted one within the strip of M-polyhedra. The bond length distortion amounts $\approx$ 7.8 % for the samples Ri1 and Ri15. Whereas the M4-O4 and M4-O2 bond lengths of this study

are close to the bond length found in literature (*e.g.* Papike *et al.*, 1969), the M4-O6 and M4-O5 bond lengths of the samples Ri1 and Ri15 are 3 – 4.0 % longer as in the potassic richterite, given in Papike *et al.* (1969). There are also pronounced differences in M4-O bond length between the Ri1 and Ri15 samples and those in the KK-richterite of Yang *et al.* (1999). These differences in the M4-O interatomic distances (especially M4-O5 and M4-O6) of the samples Ri1 and Ri15 and those given in the literature (*e.g.* Papike *et al.*, 1969; Cameron *et al.*, 1983; Yang *et al.*, 1999) can be ascribed to the different M4 site compositions and the different tetrahedral kinking angles (O5-O6-O5 angles). The tetrahedral chains in Ri1 and Ri15 yield less kinking as compared to the literature data. This effect shortens the M4-O5 bonds and drags out the M4-O6 bonds.

Cooling down to 110 K results in a decrease of the <M4-O> by 0.31 %. The largest change upon cooling is observed for the M4-O6 bond lengths, which decrease by 0.75 % between 298 K ... 110 K. The M4-O5 bond length slightly increases by 0.25 %. The decrease of the M4-O6 bond length and the increase of the M4-O5 bond length upon cooling can be ascribed to the altered tetrahedral chain kinking angle, which is 0.8° smaller at 110 K as compared to 298 K.

The A site is a large cavity situated between two back-to-back tetrahedral chains. It is occupied by potassium and minor sodium in Ri1 and by potassium in Ri15. At room temperature the K-atom appears to have a rather anisotropic electron density contribution. This applies for both samples. Cation disorder at the A site in the amphiboles has been the subject of several studies (*e.g.* Hawthorne *et al.*, 1996). In this study K seems to preferred the A(2/m) site in both samples Ri1 and Ri15. Strong thermal disorder of K is assumed. Upon cooling <U^2> values for potassium are halved but still remain strongly anisotropic. As for 298 K the split model with a distribution of potassium over an A(m) site with (x, ½, y) and an A(2) site with (0, y, 0) did not work (at least not with the programs used) at 110 K for Ri.

Conclusion

(1) In close agreement with the literature, the structure refinements on samples Ri1 and Ri15 (potassic-ferri-ferrorichterites) show that the M1 oxygen octahedron is the most regular M site polyhedron in terms of bond and edge lengths distortion and in terms of quadratic octahedral angle variance. The M3 sites exhibit a similar regular character. However, bond angle variance is somewhat larger as compared to the M1 site. The M2 site octahedron appears to be the most distorted one. This is important with respect to the Mössbauer spectroscopic results.

(2) Upon cooling from 298 K to 110 K, the tetrahedra behave very rigidly and show no significant changes in bond lengths and bond angles. The <M-O> bond lengths of the M1, M2 and M3 sites decrease by 0.19 %, 0.24 % and 0.24 % respectively. The <M4-O> bond length decreases by 0.3 % and thus is most expansible as a function of temperature. The different thermal polyhedral expansion between C-type M sites and the SiO_4 tetrahedra is accommodated by an increasing tetrahedral double-chain kinking towards lower temperatures.

(3) Mössbauer spectra show that the hydrothermally grown potassic-ferri-ferrorichterites partly contain rather high ferric iron contents up to 42 % of total iron, depending on the redox conditions at the experiment. Ferric iron strongly prefers the M2 site, only minor Fe^{3+} was found on the M3 and M1 sites. It is assumed that samples are balanced in charge by the iron-oxy reaction with a split off of protons as demonstrated by Popp *et al.* (1995).

(4) Ferric iron on the M2 site obviously introduces significant electronic and/or geometric distortions to the neighboring M1 and M3 sites. This is clearly demonstrated by the dependence of the size of ferrous quadrupole splitting on M1 and M3 on the mean ionic radius of the M2 cation (Figure 3c). The observed decrease of ferrous quadrupole splitting on M1 and M3 with increasing Fe^{3+} content is in agreement with the well known negative correlation between Fe^{2+} quadrupole splitting and site distortion (Ingalls, 1964; Dowty & Lindsley, 1973). Thereby the decreasing size of the mean ionic radius on the M2 site seems to introduce larger local geometric distortions to the M3 site, "sandwiched" between two neighboring M2 sites within the b – c plane, as compared to the M1 site. The ferrous quadrupole splitting of the M3 site decreases more rapidly with decreasing ionic radius of the M2 site as the one of the M1 site.

(5) As a direct consequence from the above findings, the difference between the quadrupole splitting of Fe^{2+} on M1 and M3 becomes larger with increasing ferric iron concentration on M2. As the potassic-ferri-ferrorichterites, investigated here, all contained significant amounts of ferric iron (Fe^{3+}/Fe_{tot} > 0.2), it was possible, to differentiate between Fe^{2+} on the M1 and M3 sites. For lower Fe^{3+} contents, a clear differentiation between Fe^{2+} on M1 and M3 probably becomes very problematic. Furthermore, based on the – admittedly somewhat speculative – findings of Figure 3c, it seems to be impossible to differentiate between Fe^{2+} on M1 and M3 for Fe^{3+}/Fe_{tot} < 0.1. Additional data for synthetic amphiboles with variable ferric iron contents would be of special interest within this context.

References

Bancroft, M.C. & Brown, J.R. (1975) A Mössbauer study of coexisting hornblendes and biotites. *Am. Mineral.*, **60**, 265–272.

Bancroft, M.C. & Burns, R. (1969): Mössbauer and absorbtion spectral study of alkali amphiboles. *Mineral. Soc. Amer. Spec. Pap.*, **2**, 137–148.

Burns, R.G. & Greaves, C. (1971): Correlations of infrared and Mössbauer site population measurements of actinolites. *Am. Mineral.*, **56**, 2010–2033.

Cameron, M., Sueno, S., Papike, J.J., Prewitt, C.T. (1983): High temperature crystal chemistry of K and Na fluor-richterites. *Am. Mineral.*, **68**, 924–943.

Charles, R.W. (1975): The phase equilibria of richterite and ferro-richterite. *Am. Mineral.*, **60**, 367–374.

Della Ventura, G., Robert, J.-L., Bény, J.-M., Raudsepp, M., Hawthorne, F.C. (1993): The OH-F substitution in Ti-rich potassium richterite: Rietveld structure refinement and FTIR and micro-Raman spectroscopic studies of synthetic amphiboles in the system K_2O-Na_2O-CaO-MgO-SiO_2-TiO_2-H_2O-HF. *Am. Mineral.*, **78**, 980–987.

Dowty, E. & Lindsley, D.H. (1973): Mössbauer spectra of synthetic hedenbergite – ferrosilite pyroxenes. *Am. Mineral.*, **58**, 850–868.

Ernst, W.G. & Wai, C.M. (1970 Mössbauer, infrared, X-ray and optical study of cation ordering and dehydrogenation in natural and heat treated sodic amphiboles. *Am. Mineral.*, **55**, 1226–1258.

Eugster, H. & Wones D.R. (1962) Stability relations of the ferruginous biotite, annite. *J. Petrol.*, **3**, 82–125.

Gottschalk, M. & Andrut, M. (1998): Structural and chemical characterization of synthetic (Na,K)-richterite solid solutions by EMP, HRTEM, XRD and OH-valence vibrational spectroscopy. *Phys. Chem. Minerals*, **25**, 101–111.

Hawthorne, F.C. (1982): Crystal chemistry of amphiboles. *Mineral. Soc. Amer., Rev. Mineral.*, **9A**, 1–102.

– (1983): The crystal chemistry of amphiboles. *Can. Mineral.*, **21**, 173–480.

Hawthore, F.C.,Oberti, R., Sardone, N. (1996): Sodium at the A site in clinoamphiboles: the effects of composition on patterns of order. *Can. Mineral.*, **34**, 577–593.

Ingalls, R. (1964): Electric-field gradient tensor in ferrous compounds. *Phys. Rev.*, **133**, A787–795.

Leake, B., Woolley, A.R., Arps, C.E.S., Birch, W.D., Gilbert, M.C., Grice, J.D., Hawthorne, F.C., Kato, A., Kisch, H.J., Krivivivhev, V.G., Linthout, K., Laird, J., Mandarino, J., Maresch, W.V., Nickel, E.H., Rock, N.M.S., Schumacher, J.C., Smith, D.C., Stephenson, N.C.N., Ungaretti, L., Whittaker, E.J.W., Youzhi, G. (1997): Nomenclature of amphiboles: Report of the subcommitee on amphiboles of the International Mineralogical Association, Commission on new minerals and mineral names. *Am. Mineral.*, **82**, 1019–1037.

Oberti, R., Ungaretti, L., Cannillo, E., Hawthorne, F.C. (1992): The bahaviour of Ti in amphibole: I. four- and six-coordinate Ti in richterite. *Eur. J. Mineral.*, **4**, 425–439.

Papike, J.J., Ross, M., Clark, J.R. (1969): Crystal chemical characterisation of clinoamphiboles based on five new structure refinements. *Mineral. Soc. Amer. Spec. Pap.*, **2**, 117–136.

Popp, R.K., Virgo, D., Hoering T.C., Yoder, H.S. Jr., Phillips, M.W. (1995): An experimental study of phase equilibria and iron oxy-component in kaersutitic amphibole: Implication for fH_2 and fH_2O in the upper mantles. *Am. Mineral.*, **80**, 534–548.

Rancourt, D.G., McDonald, A.M., Lalonde, A.E., Ping, J.Y. (1993): Mössbauer absorber thickness for accurate site populations in iron-bearing minerals. *Am. Mineral.*, **78**, 1–7.

Rancourt, D.G. & Ping, J.Y. (1991): Voigt-based methods for arbitrary-shape static hyperfine parameter distributions in Mössbauer spectroscopy. *Nuclear Instr. Meth. Phys. Res.*, **B 58**, 85–97.

Rancourt, D.G., Ping, J.Y., Boukili, B., Robert J.L. (1996): Octahedral-site quadrupole splitting distributions from Mössbauer spectroscopy along the (OH,F)-annite join. *Phys. Chem. Minerals*, **23**, 63–71.

Raudsepp, M., Della Ventura, G., Hawthorne, F.C., Robert, J.L. (1992): Powder diffraction data for synthetic potassium-richterite, nickel-potassium richterite, and cobalt-potassium-richterite. *Powder Diffraction*, **7**, 52–55.

Raudsepp, M., Turnock, A.C., Hawthorne, F.C. (1991): Amphibole synthesis at low pressure: what growth and what doesn't. *Eur. J. Mineral.*, **3**, 983–1004.

Redhammer, G.J., Amthauer, G., Lottermoser, W., Treutmann, W. (2000): Sythesis and structural properties of clinopyroxenes of the hedenbergite $CaFe^{2+}Si_2O_6$-aegirine $NaFe^{3+}Si_2O_6$ solid-solution series. *Eur. J. Mineral.*, **12**, 105–120.

Renner, B. & Lehmann, G. (1986) Correlation of angular and bond lengths distortion in TO_4 units in crystals. *Zeit. Kristall.*, **175**, 43–59.

Robert, J.-L., Della Ventura, G., Raudsepp, M., Hawthorne, F.C. (1993): Rietveld structure refinement of synthetic strontium-rich potassium-richterites. *Eur. J. Mineral.*, **5**, 199–206.

Robert, J.-L., Della Ventura, G., Thauvin, J.-L. (1989): The infrared OH-streching region of synthetic richterites in the system Na_2O-K_2O-CaO-MgO-SiO_2-H_2O-HF. *Eur. J. Mineral.*, **1**, 203–211.

Robinson, K., Gibbs, G.V., Ribbe, P.H. (1971) Quadratic elongation, a quantitative measure of distortion in coordination polyhedra. *Science*, **172**, 567–570.

Rodrigues-Carvajal, J. (1998) FULLPROF: Rietveld, profile matching and integrated intensity refinement of X-ray and/or neutron data (PC-version). Version 3.5d.

Sergent, J., Robert, J.-L., Boukili, B., Della Ventura, G. (1997): Effect of X_{fe} and fO_2 on the FTIR and Mössbauer spectra of richterites in the system K_2O-Na_2O-CaO-MgO-FeO-Fe_2O_3-TiO_2-SiO_2-H_2O. *Phys. Chem. Minerals*, **24**, 308.

Shannon, R.D. (1970) Revised values of effective ionic radii. *Acta Cryst.*, **B26**, 1046–1048.

Shannon, R.D., Prewitt, C.T. (1969) Effective ionic radii in oxides and fluorides. *Acta Cryst.*, **B25**, 925–934.

Sheldrick, G. (1993): A program for refining crystal structures. University of Göttingen, Germany.

Stoe & Cie (1996): X-SHAPE and X-RED: Programs for optimization pf the crystal shape (w.r.t. the merging R-value) and numerical absorbtion correction. Stoe & Cie.

Virgo, D. (1974): Preliminary fitting of ^{57}Fe Mössbauer spectra of synthetic Mg-Fe richterites. *Carnegie Institute of Washington Yearbook*, **73**, 513–516.

Yang, H., Konzett, J., Prewitt, C.T., Fei, Y. (1999): Single crystal structure refinement of synthetic M4 K-substituted potassic richterite $K(KCa)Mg_5Si_8O_{22}(OH)_2$. *Am. Mineral.*, **84**, 681–684.